LOCALIZED SECONDARY INSTABILITIES OF VELOCITY STREAKS IN PLANE CHANNEL FLOW

Fredrik Lundell
Dept. of Mech., KTH,
S-100 44 Stockholm, Sweden
fredrik@mech.kth.se

ABSTRACT

Secondary, wavy, instabilities of velocity streaks are studied in a plane channel flow. As opposed to previous studies, a random signal was used to force the secondary instability (at a fixed streamwise position). Momentary, the random signal exhibits specific frequencies. Eventually the frequency will be amplified by the streak, forming a (localized) growing secondary instability with a length of a few wavelengths. Earlier work, theoretical, numerical and experimental alike, have studied the streamwise growth of infinite long harmonic oscillations. If amplified by the streak, the short localized secondary disturbances might ultimately develop into a turbulent spot. Phase-averaged hot-wire measurements, together with proper evaluation of the data, gives information of the disturbances. The amplitude of the localized disturbances grow exponentially. It is indicated that the growth rate of the disturbance decreases as the length of the disturbance decreases. It is also seen that the propagation speed of the disturbances are close to the local velocity at the position where the maximum disturbance energy appear.

INTRODUCTION

It is known from flow visualizations and measurements that, assumed the disturbance amplitude of the environment is high, laminar-turbulent transition might be preceded by the formation and growth of streamwise streaks with alternating high and low velocity (Kendall (1998) , Matsubara & Alfredsson (2001)). The growth mechanism for those streaks is so called *transient growth* (Ellingsen & Palm (1973), Landahl (1980), Butler & Farrell (1992), Andersson *et al.* (1999), Luchini (2000)). Further downstream, breakdown occurs due to wave-like secondary instabilities of the streaks. For a Blasius boundary layer, this transition scenario is dominant for free-stream turbulence levels

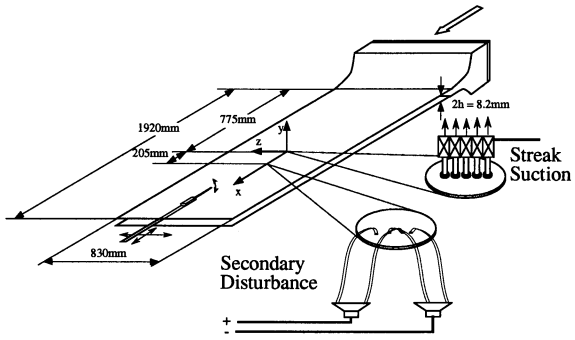

Figure 1: Experimental set-up.

ranging from about 1% to 7%. With lower disturbance levels, TS-waves interact with the streaks giving a more complex transition scenario; with higher disturbance levels turbulent spots can be produced directly by disturbances injected locally in the boundary layer by the free-stream turbulence.

Secondary instabilities of velocity streaks, modeling the instabilities of streaks appearing in free-stream turbulence induced transition, have been studied experimentally by e.g Elofsson *et al.* (1999) and Asai *et al.* (1999). Recent theoretical work has been performed by Andersson *et al.* (2001). In general, a velocity streak in a shear flow can be either stable, subject to a growing *symmetric* disturbance due to the inflectional *normal* velocity profile or subject to a growing *anti-symmetric* disturbance appearing due to the inflectional *spanwise* velocity profile. Flow visualization pictures and theory indicate that the secondary instability amplified by streaks in a laminar boundary layer are anti-symmetric, consequently driven by the spanwise inflection point.

All experiments and theory cited above have investigated infinite long, continuous wave trains. In the present work, a random forcing, simulating a turbulent free-stream forcing streaks in a laminar boundary layer, have been used. The downstream development of the thus occurring, localized secondary distur-

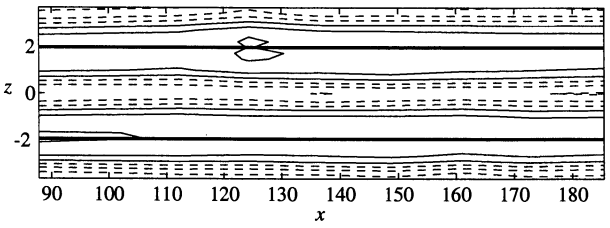

Figure 2: Mean flow variation in the xz-plane at $y = 0.36$. Contour levels are 10% of the centreline velocity, U_{CL} and negative contours are dashed. The thick solid lines shows the area showed in figures 5 & 6.

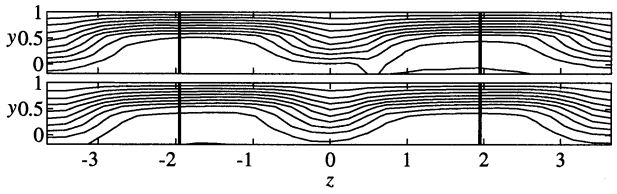

Figure 3: Mean flow variation in the upper half of the channel at $x = 112$ (top) and $x = 161$ (bottom). Contour lines are 10% of U_{CL}. As in figure 2, the thick solid lines show the area studied in figures 5 & 6.

bances have been studied. In a real boundary layer undergoing transition, flow visualizations show that the secondary instabilities occurring naturally indeed have a length of a few wavelengths only.

The process sketched above, growth of streamwise streaks followed by the amplification of secondary instabilities and finally breakdown, is also believed to be the process behind the growth and bursting of streaks in turbulent, wall bounded shear flows.

EXPERIMENTAL SET-UP

The set-up shown in figure 1 was used. The flow apparatus is a plane channel, consisting of two glass plates separated by 8.2 mm thick aluminium bars. The air is blown through the channel by a centrifugal fan and before the channel, the air passes a silencer, a stagnation chamber with two turbulence damping screens and finally a plane contraction before entering the channel region. The aspect ratio of the channel is 1:100 and the first instrumental plug is positioned 95 channel heights downstream of the channel inlet.

A single hot-wire can be traversed to any point in the flowfield. The hot wire measures the streamwise velocity component.

In the channel, five laminar streamwise velocity streaks are generated by applying suction through streamwise slots at one of the channel walls. At first, the streaks grow rapidly and reaches a maximum amplitude, whereupon they decay slowly downstream. The spanwise wavelength of the streaks were 15 mm.

The coordinates are x, y and z for the streamwise, wall-normal and spanwise direction, respectively. All lengths are normalized with the half-channel height h and the origin is positioned at the centre of the channel. The spanwise position of the origin is at the centre of a low velocity streak; the streamwise position of the origin is at the position of streak generation.

In figure 2 the streaks are shown in the xz-plane at $y = 0.36$, i.e. approximately one third towards the upper wall from the centre of the channel. Once established, the secondary disturbances have their maximum amplitude at this height. The contours show the velocity after subtraction of the spanwise mean at each x. As seen in the figure, the streaks are fairly independent of x. The peak-to-peak amplitude is approximately 55% of the centreline velocity.

The yz-distribution of the streaks at $x = 112$ and 161 are shown in figure 3. Note that $y = 0$ and 1 corresponds to the centre and upper wall of the channel, respectively, i.e. only the upper half of the channel is shown. To be able to show the velocity distribution up to the wall at $y = 1$, the velocity was interpolated to zero at the wall. The measurements extend to $y = 0.75$.

The disturbance generation of the present experiment is inspired by the experiment of Shaikh (1997), who generated turbulent spots in a boundary layer using random, but repeatable suction/blowing through a hole in the plate. The streaks io the channel are susceptible of a secondary instability, which in the present work was forced by blowing/suction through spanwise slots driven by speakers connected to the slots by PVC-tubes. The streamwise position of the slots is $x = 50$. The speakers were driven by random but repeatable noise in a suitable frequency band. Two speakers, driven with the original and inverted signal, respectively, were used. By connecting tubes from the two speakers to different slots, symmetric and anti-symmetric modes of the secondary instability could be forced. In the present set-up, anti-symmetric disturbances are much stronger amplified than symmetric ones.

The centreline velocity U_{CL} is used for velocity normalization. During the reported measurements, the centreline velocity was constant within $\pm 1.5\%$ and equal to 13.5 m/s,

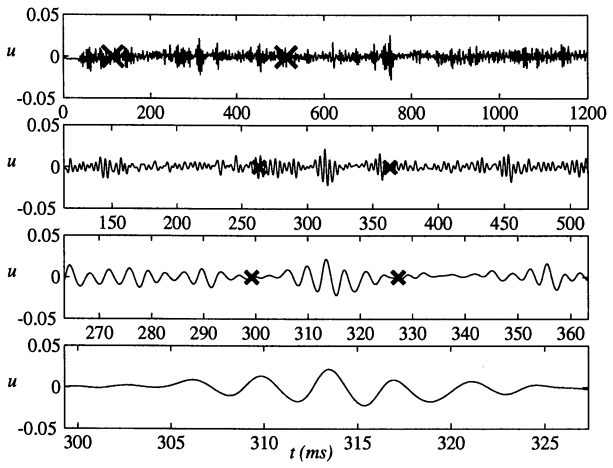

Figure 4: Phase averaged velocity signal from $y = 0.36$, $z = -0.49$. Top figure shows the full sequence and the following figures zoom in on the period marked with crosses in the figure above.

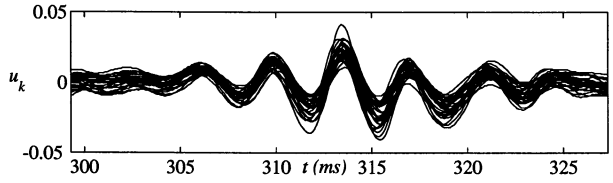

Figure 5: The 30 realizations averaged for the last trace in figure 4.

giving a Reynolds number defined as $Re = U_{CL}h/\nu$ of 3700. The critical Reynolds number is 5772, so all single-mode disturbances were damped in the channel.

Measurements were performed at 9 streamwise, 7 vertical and 31 spanwise positions. The secondary instability forcing was driven with a 1 s long, predetermined random sequence, digitally bandpass filtered between 100 and 500 Hz (the most amplified frequency was around 260 Hz). At each position, the sequence was run 20 times, allowing phase averaging in order to investigate repeated and intermittent features of the generated disturbance. The amplitude of the secondary instability forcing was chosen so that a few (3-7) turbulent spots appeared at the most downstream measurement positions during one realization of the disturbance sequence. In the present paper, repeated features of the disturbances are reported.

The velocity U is decomposed into a mean part, as shown in figures 2 & 3, and a fluctuating part, denoted u, including the time dependent secondary instability together with momentary changes of the velocity distribution due to turbulent spots.

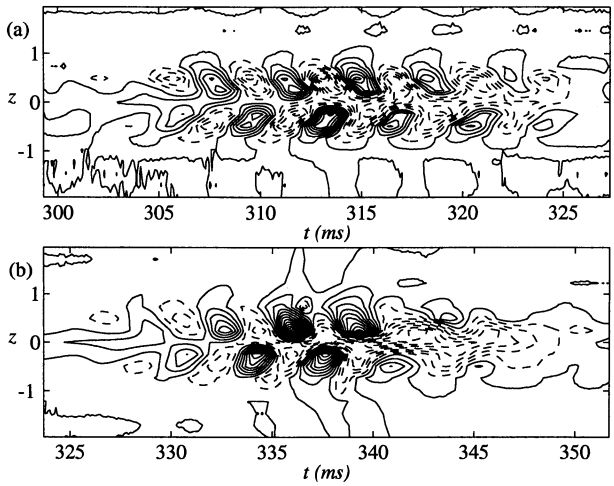

Figure 6: Phase averaged disturbance velocity u at $x = 161$, $y = 0.36$. Contour levels are 0.3% and 1% of U_{CL} in (a) and (b), respectively. Negative contours are dashed.

RESULTS AND DISCUSSION

An example disturbance

A phase-averaged velocity signal from $(x, y, z) = (112, 0.36, -0.49)$ is shown in figure 4. From the top and down, the signal is zoomed in on a single, localized secondary disturbance, occurring where it does since the secondary instability forcing had a momentary high energy content around an amplified frequency.

In the top trace of figure 4, quite a few strong oscillations of the velocity are seen, especially around $t = 300$ ms and $t = 750$ ms. Zooming in around $t = 300$ ms, to the second trace from the top in the figure, the oscillations are seen in more detail. For the eye, the strong oscillations seem to be of constant frequency (later, more detailed studies of the phase-averaged velocity will show that the frequency varies approximately $\pm 20\%$ for the different identified disturbances). The trace also shows that the higher amplitude oscillations are of various lengths; some consists of one or two periods only, whereas other can persist for seven oscillations or more. The third and fourth trace in figure 4 continues the zooming, finally showing a single, isolated disturbance at the bottom.

In figure 5, the 30 individual realizations averaged in figure 4 are shown. The zero-level of the traces are seen to vary slightly (approximately $\pm 0.7\%$ of U_{CL}) around the mean value. The oscillation is due to the large values of $\partial u/\partial y$ and $\partial u/\partial y$ at the position of the hot wire. Apart from this oscillation, small but distinct variations in phase, amplitude and fre-

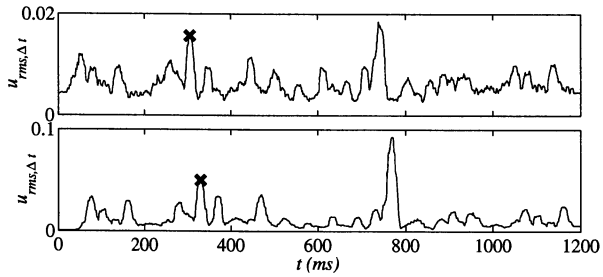

Figure 7: Time trace of $u_{rms,\Delta t}$ defined by equation (1). The centre of the disturbance studied in figures 5, 6 & 9 is marked with a cross.

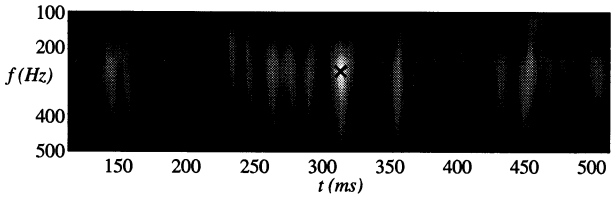

Figure 8: The wavelet transform of the second signal from the top in figure 4. Black is the minimum value whereas white is maximum. The cross marks the time of maximum $u_{rms,\Delta t}$ and the frequency at which the energy is maximum of the disturbance studied in figure 5, 6 & 9.

quency are present.

The velocity distribution measured by the hot wire as the disturbance passes is shown in figure 6. The disturbance is shown as contours of streamwise velocity in a zt-plane, showing the bottom trace of figure 4 together with the traces from other spanwise positions. The five periods seen in the bottom trace of figure 4 are clearly seen as six positive peaks following a line of constant $y = 0.49$. The spanwise extent shown in figures 6 are shown with the solid lines in figures 2 and 3. Note that the time of occurrence is later in figure 6 (b), since the disturbance reaches the downstream position later than the upstream position shown in figure 6 (a). The contour levels are three times larger in figure 6 (a) as compared to (b), due to the streamwise growth of the disturbance. Comparing the two distributions in detail, the downstream distribution is more centralized around the maximum peak whereas the amplitude is high for a longer period at the upstream position in (a). The individual peaks are also seen to move towards $z = 0$ as they propagate downstream.

Disturbance properties

In order to study the amplitude development of disturbances such as the one shown above, a local measure of the velocity oscillations was defined as:

$$u_{rms,\Delta t}(t,x) = \max_{y,z} \sqrt{\frac{1}{\Delta t}\int_{t-\Delta t/2}^{t+\Delta t/2} u^2(t,x,y,z)dt}. \quad (1)$$

In the present study, an integrating period Δt of 16 ms was used. This was the shortest period giving a $u_{rms,\Delta t}(t,x)$ with a single, well-defined, peak for each localized disturbances.

The temporal development of $u_{rms,\Delta t}$ at $x =$ (top) and 161 (bottom) are shown in figure 7. The disturbance introduced in figures 4–6 occurs at $t \approx 320$ ms and is marked with a cross. In the upper plot, it is seen that $u_{rms,\Delta t}$ exhibits distinguishable maxima at certain times. In the plot below, it is seen that the amplitude of these peaks increase downstream, even though the amplification is different from one peak to the other. When comparing the two traces in figure 7, the previously mentioned shift to later times downstream is clearly seen. However, there is no difficulty to identify peaks corresponding to the same disturbance at the two positions. From the calculated $u_{rms,\Delta t}(t,x)$, the time of appearance, $t_i(x)$ of single disturbances can be determined at different streamwise positions, together with the corresponding amplitude $u_{rms,\Delta t,i}(x)$.

In order to determine the momentary frequency of the disturbances, wavelet analysis was used. The wavelet transform of the signal shown in figure 4 is shown in figure 8. The time excerpt in figure 8 is the same as in the second from the top in figure 4. In figure 8, the Morlet wavelet transform is shown, white indicating high energy. A peak in the wavelet transform means that the signal oscillates strongly at the time and with the frequency indicated by the peak. In the present case, a number of peaks, corresponding to the disturbance known from figures 5 & 6 (as usual marked with a cross) and its neihgbouring disturbances (see figure 7) are seen. With the time of occurrence of a disturbance known from the analysis of $u_{rms,\Delta t}(t,x)$, the corresponding frequency is easily determined as the frequency at which the wavelet transform exhibits a maximum for that time.

The duration, τ_i, of a disturbance is defined as the time during which $u_{rms,\Delta t}(t,x)$ stays over a threshold value around the time at which the disturbance appears. The threshold value was chosen to be 89% of the value of $u_{rms,\Delta t}$ at t_i (i.e. when the disturbance energy, u^2, had dropped to 80% of its maximum value). Concluding, the duration τ_i of the ith disturbance appearing at $t = t_i$ is defined by

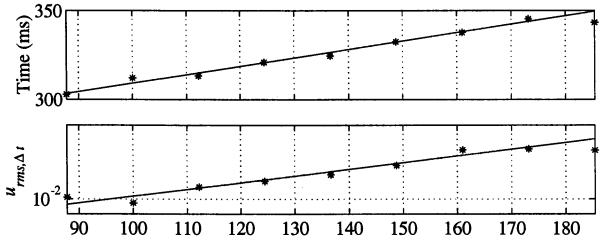

Figure 9: Streamwise development of time of occurrence t_i, frequency maximizing the wavelet energy f_i, $u_{rms,\Delta t,i}$ and τ_i, defined by equation (2) from the top and down, respectively. The disturbance under study is shown introduced in figures 4–6.

the maximum τ_i for which

$$u_{rms,\Delta t}{}^2(t) > 0.8 u_{rms,\Delta t}{}^2(t_i) \quad \text{where} \quad t \in [t_i - \alpha\tau_i, \quad t_i + (1-\alpha)\tau_i]\,. \tag{2}$$

The value of the parameter α ranges from 0 to 1, depending on the exact shape of $u_{rms,\Delta t}(t)$ around $t = t_i$. Now, four properties of the disturbance have been determined: its time of occurrence $t_i(x)$, amplitude $u_{rms,\Delta t,i}(x)$, frequency $f_i(x)$ and duration $\tau_i(x)$.

The streamwise development of the amplitude and time of occurrence for the example disturbance are shown in figure 9. From the time of occurrence, the disturbance is seen to propagate downstream with constant speed. The early time at the downstream end of the channel is due to the development of a turbulent spot, propagating *slower* than the initial, oscillating disturbance. From the time of occurrence at different streamwise positions, the propagation velocity $u_{p,i}$ of the disturbance is easily determined.

Figure 9 clearly shows that the amplitude, $u_{rms,\Delta t,i}$ grows exponentially, as expected for a disturbance following linear dynamics. The slope of the line defines the growth factor, γ. This specific disturbance is seen to grow slightly more than 10 times passing the test section.

The momentary frequency and duration for a specific disturbance did not vary considerably at different streamwise positions.

Properties of different disturbances

As was seen in the plot of the localized disturbance amplitude, $u_{rms,\Delta t}(t)$, there are a number of distinguishable disturbances occurring during the measurement period. The properties defined above (i.e. time of occurrence, amplitude, frequency, duration, velocity and growth) was determined for 13 individual peaks. The results are shown in figures 10 and 11.

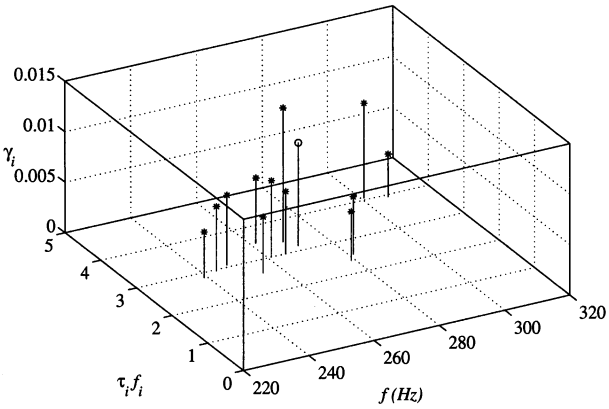

Figure 10: Streamwise growth factor γ of $u_{rms,\Delta t}(t_i)$ as a function of f_i and τ_i.

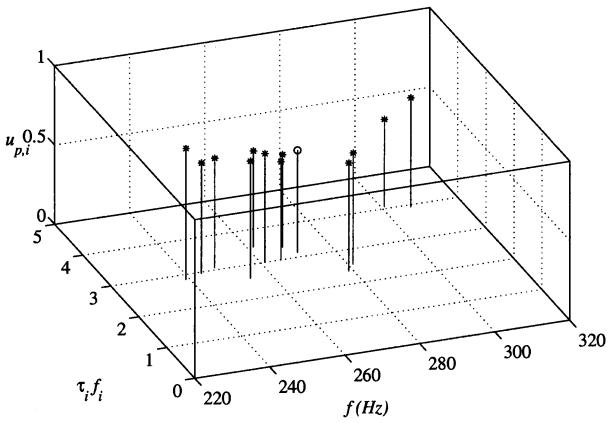

Figure 11: Streamwise propagation velocity of $max(u_{rms,\Delta t}(t_i))$ as a function of f_i and τ_i.

e

In figure 10, the exponential growth factor of the 13 identified disturbances are plotted as a function $\tau_i f_i$ (i.e. the number of periods, or wavelengths, of the disturbance) and the frequency. The disturbance used as example is marked with a ring, the others with stars.

Studying figure 10 a few features will be pointed out. The first, and most important, is that the growth of the disturbance seems to decrease as the length/duration of the disturbance decreases. The second, and less surprising, is that there exists an optimal frequency, at which maximum growth is obtained. In the present case, the frequency yielding maximum growth is around 260 Hz. For frequencies higher or lower than the frequency maximizing the growth, the growth decreases. The number of disturbances available in the present database are however far to few to draw any quantitative conclusions. Nevertheless, the qualitative trend is clear.

When it comes to the propagation velocity

$u_{p,i}$, shown in figure 11, no clear trends are seen. The propagation velocity of the maxima in $u_{rms,\Delta t}(t_i)$ is seen to be constant and roughly 65% of the centre-line velocity, a value previously obtained by Elofsson *et al.* studying a streak triggered by a continuous sinus wave in the same channel. The value is slightly lower than the local flow velocity at the y-position of the maximum of $u_{rms,\Delta t}(t, y)$.

CONCLUSIONS

Short, localized secondary instabilities of streaks have been studied. Velocity streaks were triggered by random, repeatable, noise by blowing/suction through slits in the upper channel wall. After phase averaging it was possible to determine the
(i) time of occurrence
(ii) amplitude
(iii) frequency
(iv) duration
of single disturbances, a few wavelengths long. It could be concluded that short disturbances grew slower than long, whereas the propagations speed was fairly constant. Due to the few disturbances available in the dataset (13), no quantitative conclusions could be made.

Acknowledgment

Professor Henrik Alfredsson is gratefully acknowledged for discussions, enthusiastic encouragement throughout the work and comments on the manuscript. Mr. Marcus Gällstedt and Mr. Ulf Landn are gratefully acknowledged for skillful help and instructions in the workshop.

References

Andersson, P., Berggren, M. & Henningson, D. S. 1999, "Optimal disturbances and bypass transition in boundary layers", *Phys. Fluids.* **11** pp. 134–150

Andersson, P., Brandt, L., Bottaro, A. & Henningson, D. S. 2001 "On the breakdown of boundary layer streaks", *J. Fluid Mech.* **428** pp. 29–60

Asai, M., Minagawa, M. & Nishioka, M. 2000 "Instability and breakdown of the three-dimensional high-shear layer associated with a near-wall low-speed streak", in *Laminar-Turbulent Transition*, Fasel, H. F. & Saric, W. S., ed. Springer Verlag, Berlin, pp. 269–274

Butler, K. M. & Farrell, D. F. 1992, "Three dimensional optimal perturbations in viscous shear flow", *Phys. Fluids A* **4**, pp. 1637–1650

Ellingsen, T & Palm, E. 1975, "Stability of linear flow", *Phys. Fluids.* **18**, p. 487

Kendall, J. M. 1998, "Experiments on boundary layer receptivity to freestream turbulence", AIAA-paper 98-0530

Landahl, M. T. 1980, "A note on an algebraic instability of inviscid shear flows", *J. Fluid Mech* **98**, pp. 243–251

Luchini, P. 2000, "Reynolds number independent instability of the boundary layer over a flat surface: optimal perturbations", *J. Fluid Mech.* **404** pp. 289–309

Matsubara, M. & Alfredsson, P. H. 2001, "Disturbance growth boundary layers subjected to free-stream turbulence", *J. Fluid Mech.* **430** pp.149–168

Shaikh, F. N. 1997, "The generation of turbulent spots in a laminar boundary layer", *Eur. J. Mech/B Fluids* **16** pp. 349–385 pp 29-60